A Magnus Theory

H. R. VAUGHN* AND G. E. REIS†
Sandia Laboratories, Albuquerque, N. Mex.

An analytical method is developed for predicting Magnus force and moment coefficients for spinning ogive cylinders, cone cylinders, and conical bodies in laminar compressible flow. The contributions to the Magnus coefficients due to boundary-layer displacement thickness distortion and radial pressure gradient effects are included. The boundary-layer theoretical model, which agrees well with experimental boundary-layer velocity profiles, was obtained by applying a compressibility correction and transformations to the Blasius flat plate solution to account for the effects of body shape, angle of attack, and spin. The Magnus theory is shown to agree favorably with experimental data.

Nomenclature

C_P = pressure coefficient
$C_{n_{pa}}$ = Magnus moment coefficient
$C_{Y_{pa}}$ = Magnus force coefficients [Eq. (63)]
d = afterbody diameter
f' = Blasius function [Eq. (21)]
F_Y = lateral Magnus force
h = defined by Eq. (57)
H = defined by Eq. (76)
k = compressibility correction
l = body length
L = normalized length = l/d
m = Mangler transformation
M = Mach number
p = spin rate
P = pressure
r = radius
Re_l = Reynolds number based on l and freestream conditions
Re_x = Reynolds number based on x and freestream conditions
Re_∞ = unit Reynolds number
T = temperature
v_x = longitudinal velocity
v_r = radial velocity
v_ϕ = circumferential or tangential velocity
V_c = cone surface velocity
V_∞ = freestream velocity
x = longitudinal distance from nose
y = distance normal to body surface = $r - r_b$
α = angle of attack, radians
β = compressibility factor [Eq. (30)]
δ = boundary-layer velocity thickness ($f' = 0.99425$)
δ^* = boundary-layer displacement thickness
η = boundary-layer thickness parameter
μ = viscosity
ρ = density
ϕ = circumferential angle
Φ^* = velocity potential at boundary-layer displacement thickness

Subscripts and Superscripts

a = afterbody
aw = adiabatic wall
b = local body conditions
c = cone or cylinder
cc = cone-cylinder
e = edge of boundary layer
i = inviscid
l = body length
n = nose
o = ogive
oc = ogive-cylinder
s = spherical
w = wall conditions
ω = viscosity temperature ratio exponent
1 = side 1 (advancing side)
2 = side 2 (retreating side)
∞ = freestream conditions
$(\ )'$ = average or effective conditions in boundary layer

Received December 26, 1972; presented as Paper 73-124 at the AIAA 11th Aerospace Sciences Meeting, Washington, D.C., January 10–12, 1973; revision received June 11, 1973. This work was supported by the U.S. Atomic Energy Commission.

Index category: Boundary Layers and Convective Heat Transfer—Laminar.

* Supervisor, Aeroballistics Division, Aerodynamics Project Department. Associate Fellow AIAA.

† Member of Technical Staff, Aeroballistics Division, Aerodynamics Project Department.

I. Introduction

THE importance of the Magnus moment to the stability of spin stabilized projectiles is well established by the Tricyclic Theory.[1-3] The Magnus coefficients have been investigated theoretically and experimentally by a number of authors whose work was recently summarized by Platou.[4] Previous theoretical work, notably that of Kelly-Thacker,[5] Martin,[6] and Sedney,[7] were either restricted to incompressible boundary layers[5,6] or to either a cylinder[5,6] or a cone.[7] With one exception,[5] previous work has included only the effect of the distorted boundary-layer displacement thickness resulting from combined angle of attack and spin. While this is an important contribution to the Magnus force, the effect of the radial pressure gradient in the boundary layer resulting primarily from centrifugal forces acting in the boundary layer is equally important. In the theory presented here, both these effects are included together with the effect of leeside vortices, which is accounted for by an empirical relation obtained from wind-tunnel tests.[8] While it is possible to derive the theory for many body shapes only the more common tangent ogive cylinder, cone cylinder, and conical shapes are considered. The boundary-layer model used in previous theoretical approaches has in general been obtained through a perturbation solution to the boundary-layer equations. In the present case, the boundary-layer model is obtained by analytic techniques from the Howarth and Mangler transformation, where the effect of spin and angle of attack is obtained from an additional transformation suggested by the Mangler transformation. Some of the quantities used in the development are defined in Fig. 1.

II. Boundary-Layer Model

The Howarth-Mangler transformation for a compressible laminar boundary layer on a body of revolution at zero angle of attack is[10]

$$\xi(x) = \int_0^x (\rho\mu) v_{x_e} r_b^2 \, dx \tag{1}$$

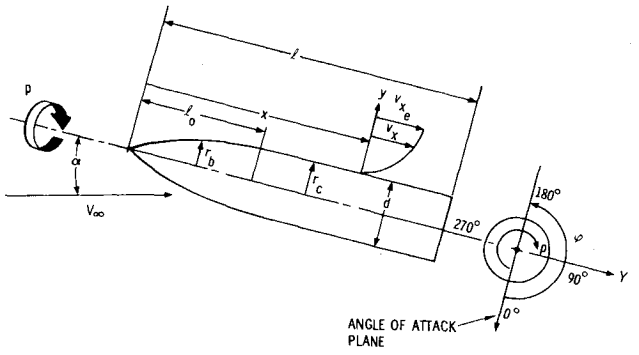

Fig. 1 Tangent ogive-cylinder and boundary-layer longitudinal velocity profile geometry.

$$\eta(x,y) = \frac{v_{x_e} r_b}{(\xi)^{1/2}} \int_0^y \rho \, dy \tag{2}$$

These equations describe the longitudinal velocity profiles of a nonspinning body of revolution at zero angle of attack in terms of the incompressible Blasius flat plate solution.[9] If it is assumed that the effects of longitudinal velocity and pressure gradients can be ignored and if the density and viscosity can be treated as average or effective values, Eqs. (1) and (2) become

$$\xi = (\rho\mu)' V_\infty \int_0^x r_b^2 \, dx \tag{3}$$

$$y = \frac{(\xi)^{1/2}\eta}{V_\infty \rho' r_b} \tag{4}$$

where the prime indicates effective values and the boundary-layer edge velocity is assumed equivalent to the freestream velocity. Substituting Eq (3) in Eq. (4) and letting

$$\rho_\infty/\rho' = T'/T_\infty, \quad \mu'/\mu_\infty = (T'/T_\infty)^\omega \tag{5}$$

$$y = \left(\frac{\eta x}{(Re_x)^{1/2}}\right)\left(\frac{T'}{T_\infty}\right)^{(1+\omega)/2}\left(\frac{\int_0^x \pi r_b^2 \, dx}{\pi r_b^2 x}\right)^{1/2} \tag{6}$$

The first term is the Blasius incompressible solution for a flat plate, the second term is the compressibility correction and the third term is Mangler's transformation‡ in a slightly altered form, which provides some insight as to its physical significance. The compressibility correction can be obtained from Eckert's work,[11] and is

$$k = T'/T_\infty = 1 + 0.0374 M_e^2 + 0.5(T_w/T_\infty - 1) \tag{7}$$

where a laminar recovery factor of 0.85 is used. For the conditions that occur in a continuously operating wind tunnel the compressibility correction can be further simplified, because the viscosity exponent ω is 1.00 in the range of wind-tunnel temperatures[9] and the wall temperature (T_w) can be approximated by the adiabatic wall temperature

$$T_w/T_\infty = T_{aw}/T_\infty = 1 + 0.17 M_e^2 \tag{8}$$

For wind-tunnel conditions then

$$k = (T'/T_\infty)^{(1+\omega)/2} = T'/T_\infty = 1 + 0.1224 M_e^2 \tag{9}$$

For the case of long bodies the edge Mach number (M_e) can be assumed to be equivalent to the freestream Mach number (M_∞) with a small error. In the case of short conical bodies, the inviscid cone surface Mach number should be used to avoid a significant error. It should be emphasized that Eq. (9) is valid only for wind-tunnel testing. In the case of flight the actual wall temperature and the ω consistent with the flight boundary-layer temperature should be used. From Eqs. (6) and (9)

$$y = [\eta x/(Re_x)^{1/2}] k m_n m_{\alpha,p} \tag{10}$$

‡ The term "Mangler's transformation" will be used here to describe both the transformation and the results of the transformation.

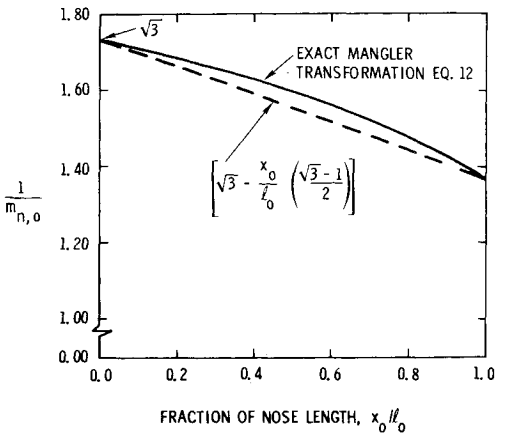

Fig. 2 Mangler transformation for ogive.

where k is the compressibility correction, m_n the Mangler transformation for the nose and $m_{\alpha,p}$ a Mangler type of transformation for angle of attack and spin. The Mangler transformation for a tangent ogive nose ($m_{n,o}$) is obtained by substituting

$$r_b = r_c[1-(1-x_o/l_o)^2] \tag{11}$$

for the local ogive radius into the Mangler transformation part of Eq. (6) where r_c is the base radius

$$m_{n,o} = \left[\frac{\int_o^{x_o} \pi r_b^2 \, dx}{\pi r_b^2 x_o}\right]_{n,o}^{1/2} = \frac{[\frac{4}{3}(x_o/l_o)^2 - (x_o/l_o)^3 + \frac{1}{5}(x_o/l_o)^4]^{1/2}}{[1-(1-x_o/l_o)^2]} \tag{12}$$

The reciprocal of Eq. (12) is compared in Fig. 2 with the linear approximation

$$m_{n,o} = \left\{(3)^{1/2} - \frac{x_o}{l_o}\left[\frac{(3)^{1/2}-1}{2}\right]\right\}^{-1} \tag{13}$$

which is sufficiently accurate to be used here. The Mangler transformation for a cylindrical afterbody is, of course, unity.

The angle-of-attack and spin transformation ($m_{\alpha,p}$) is obtained by using the physical concept contained in the normal zero angle of attack Mangler transformation. Notice [Eq. (6)] that this transformation in physical terms is the square root of the volume of the body ahead of the body station of interest divided by the cylindrical volume of the stream tube generated by the radius at the local body station of interest and length of the body ahead of

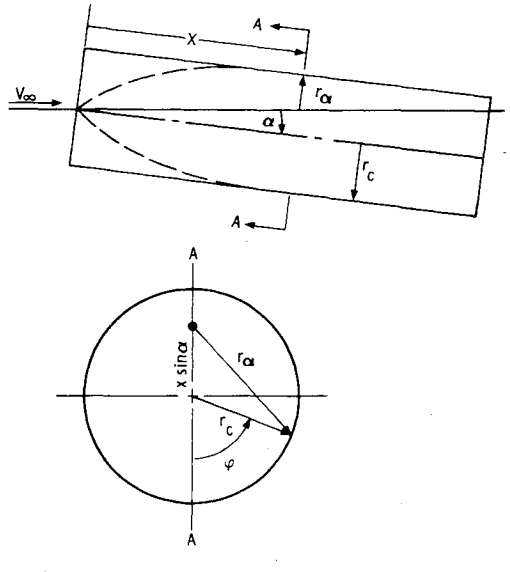

Fig. 3 Angle-of-attack transformation geometry.

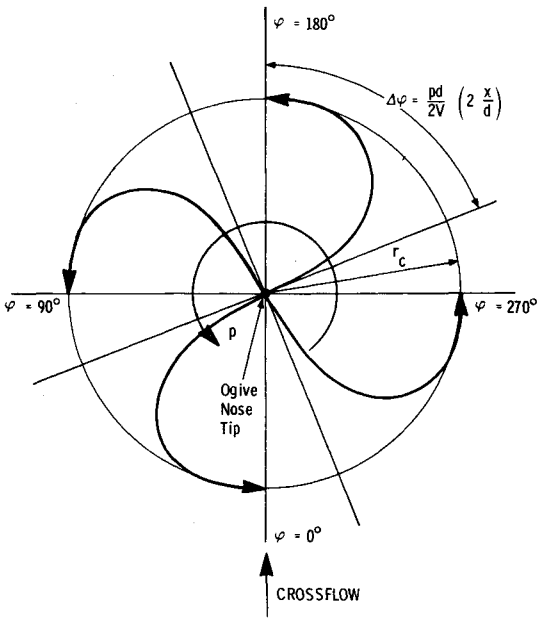

Fig. 4 Distortion of boundary-layer streamline resulting from body spin.

the local body station. Since the effect of angle of attack and spin is being superimposed on the other transformations [Eq. (10)] the body is treated as a cylinder (Fig. 3). Consequently, the Mangler transformation for angle of attack is, from the physical concept defined above, the square root of the volume of the cylindrical body ahead of the local body station divided by the stream tube volume determined by the local radius (r_α) between the freestream vector and the body surface. Then

$$m_{\alpha,p} = \left(\frac{\int_o^x \pi r_c^{\,2}\, dx}{\pi r_\alpha^{\,2} x} \right)^{1/2} = \{1 + 4[(x/d)\sin\alpha]^2 + 4[(x/d)\sin\alpha]\cos\phi'\}^{-1/2} \quad (14)$$

where r_α can be derived from the geometry shown in Fig. 3. Now, the circumferential angle (ϕ'), which is measured from the windward meridian in the direction of spin, is the effective circumferential angle that an average boundary-layer streamline would experience. Shown in Fig. 4 is the streamline path of a fluid particle moving with the longitudinal freestream velocity and the body circumferential velocity, which in effect, is an approximation of the average streamline in the boundary layer. The change in circumferential angle ($\Delta\phi$) for the average streamline then is

$$\Delta\phi = (pd/2V_\infty)(2x/d) \quad (15)$$

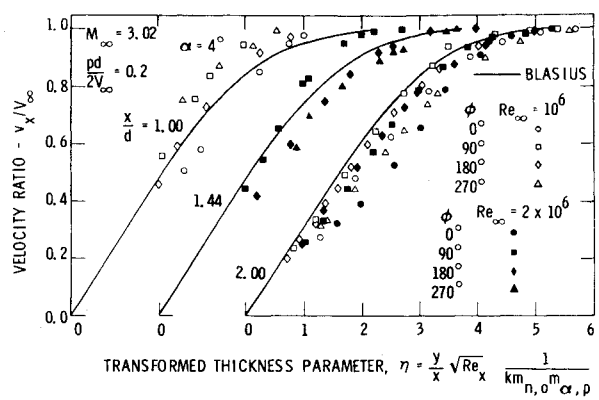

Fig. 5 Transformed nose velocity profiles for angle-of-atack case and $pd/2V_\infty = 0.2$.

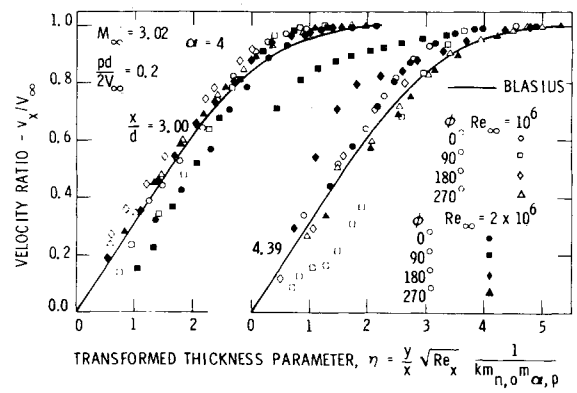

Fig. 6 Transformed afterbody velocity profiles for angle-of-attack case and $pd/2V_\infty = 0.2$.

and the effective circumferential angle ϕ' is approximated by

$$\phi' = \phi + \Delta\phi/2 = \phi + (pd/2V_\infty)x/d \quad (16)$$

where ϕ is referenced to the angle of attack plane. Substituting Eq. (16) in Eq. (14) yields

$$m_{\alpha,p} = \{1 + 4[(x/d)\sin\alpha]^2 + 4[(x/d)\sin\alpha]\cos[\phi + (pd/2V_\infty)x/d]\}^{-1/2} \quad (17)$$

which is the complete transformation for angle of attack and spin. The transformed thickness parameter obtained from Eqs. (9, 10, 13, and 17) is

$$\eta = [y(Re_x)^{1/2}/x](1/km_n m_{\alpha,p}) \quad (18)$$

The ability of this boundary-layer model to predict boundary-layer longitudinal velocity profiles is shown in Figs. 5 and 6, where experimentally determined velocity profiles[12] are plotted as a function of the transformed thickness parameter in comparison with the Blasius profile. The agreement is good, except for the rear of the body where transition to a turbulent boundary layer is occurring at the higher Reynolds number ($Re_\infty = 2\times10^6$).

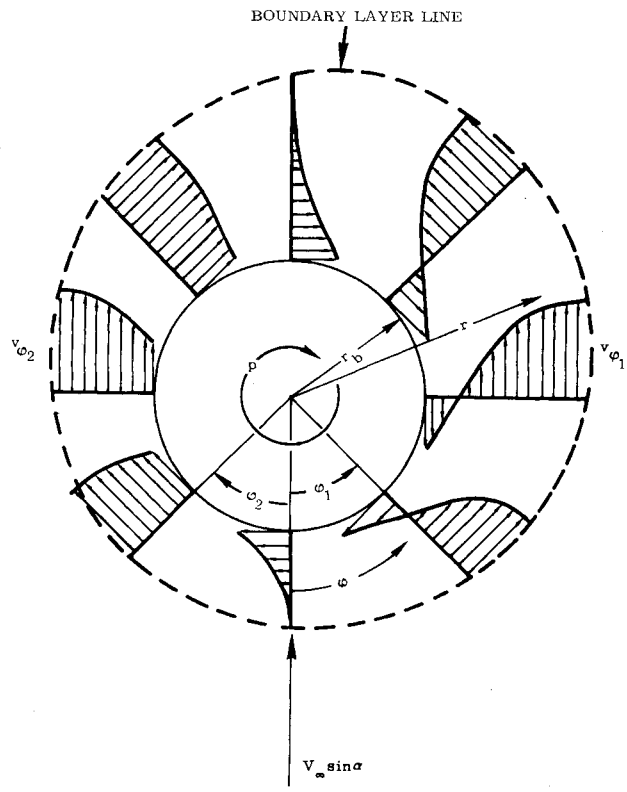

Fig. 7 Typical boundary-layer circumferential velocity profiles.

Similar comparisons of the theory and experimental data for other conditions are shown in Ref. 12.

The circumferential velocity profile (v_ϕ) is constructed by assuming a Blasius profile exists between the body surface circumferential velocity and the inviscid circumferential velocity ($v_{\phi i}$) at the edge of the boundary layer. Experimental tests[13] confirm this assumption, which when expressed in equation form is

$$v_{\phi_1} = -r_b p(1-f') + (2V_\infty \sin\alpha \sin\phi) f' \quad (19)$$

$$v_{\phi_2} = r_b p(1-f') + (2V_\infty \sin\alpha \sin\phi) f' \quad (20)$$

where f' is obtained from the Blasius solution

$$f' = \partial f/\partial\eta = v_x/V_\infty \quad (21)$$

Figure 7 shows the circumferential velocity profiles at eight circumferential angles (ϕ) and the boundary-layer thickness profile (dashed line) obtained from Eqs. (18–20) for a typical set of conditions. Note that the inviscid circumferential velocity ($v_{\phi i} = 2V_\infty \sin\alpha \sin\phi$) was obtained from potential flow theory and is valid on the nose of a projectile at small angles of attack when vortex flow has not formed. This will be compensated for in the case of vortex formation on the cylindrical afterbody later in the development.

III. Magnus Theory

There appears to be two major causes of the Magnus force which are shown in Fig. 8 as a function of Mach number. The function H, to be derived later, is directly proportional to the Magnus force coefficient. The boundary-layer distortion effect can be seen in Fig. 7 where it is evident that the boundary layer is thicker on the advancing side (i.e., side 1 where the body surface velocity advances toward the crossflow velocity) than on the retreating side (i.e., side 2 where the body surface velocity retreats from the crossflow velocity). If the boundary-layer displacement thickness (δ^*) is treated as an effective physical boundary, the effective body shape is distorted in such a manner as to cause a higher pressure to be generated on the advancing side than on the retreating side. This results in a net lateral force to the left which is one of the components of Magnus force. There is also a force component in the same direction generated by the difference in the centrifugal force acting on the boundary layer from side to side. Notice in Fig. 7 that the average circumferential velocity is greater on the retreating side (side 2) than it is on the advancing side (side 1), resulting in a larger centrifugal force acting on the boundary-layer mass on the retreating side. This and other less important effects to be considered later cause a difference in the radial pressure gradient from side to side.

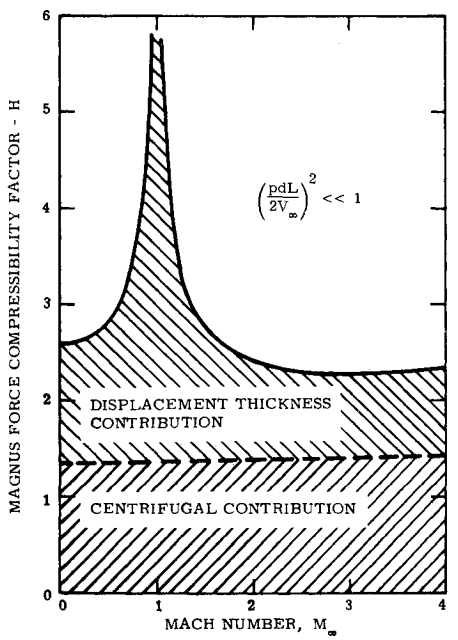

Fig. 8 Effect of compressibility on Magnus force.

The force component due to boundary-layer displacement thickness distortion is obtained by evaluating the difference in thickness from side to side from the angle-of-attack and spin transformation [Eq. (17)] which can be expanded to obtain

$$m_{\alpha,p} = 1 - 2(x/d)\sin\alpha\cos[\phi + (pd/2V_\infty)x/d] + \ldots \quad (22)$$

if $[(2x/d)\sin\alpha]^2 \ll 1$. From Eqs. (10) and (22), the difference in boundary-layer displacement thickness ($\eta = 1.72$) from side to side is

$$\delta_1^* - \delta_2^* = \delta^*(m_{\alpha,p_1} - m_{\alpha,p_2}) \quad (23)$$

where δ^* is the compressible boundary-layer displacement thickness undistorted by either angle of attack or spin

$$\delta^* = [1.72x/(Re_x)^{1/2}](T'/T_\infty)m_n \quad (24)$$

Now $m_{\alpha,p}$ for the two sides is

$$m_{\alpha,p_1} = 1 - 2(x/d)\sin\alpha\cos[\phi_1 + (pd/2V_\infty)x/d] \quad (25)$$

$$m_{\alpha,p_2} = 1 - 2(x/d)\sin\alpha\cos[\phi_2 - (pd/2V_\infty)x/d] \quad (26)$$

When Eqs. (25) and (26) are substituted in Eq. (23) and it is specified that $\phi = \phi_1 = \phi_2$ Eq. (23) becomes

$$\delta_1^* - \delta_2^* = 4(x/d)\sin\alpha\sin\phi\sin[(pd/2V_\infty)(x/d)\delta^*] \quad (27)$$

after some manipulation. The term $\sin(pd/2V_\infty\, x/d)$ can be expanded yielding

$$\delta_1^* - \delta_2^* = 4(x/d)\sin\alpha\sin\phi\,\delta^*\{(pd/2V_\infty)(x/d) - (1/3!)[(pd/2V_\infty)(x/d)]^3 + (1/5!)[(pd/2V_\infty)(x/d)]^5\} \quad (28)$$

when only the first three terms of the expansion are retained. From perturbation theory[14] the difference in pressure coefficient from side to side is

$$C_{P_1} - C_{P_2} = \frac{P_1 - P_2}{\frac{1}{2}\rho_\infty V_\infty^2} = \frac{-2(\Delta V_1 - \Delta V_2)}{\beta V_\infty} \quad (29)$$

where β is the compressibility correction.

$$\beta = (|1 - M_\infty^2|)^{1/2} \quad (30)$$

The difference in perturbation velocities from side to side is

$$\Delta V_1 - \Delta V_2 = (\partial/\partial x)(\Phi_1^* - \Phi_2^*) \quad (31)$$

where Φ^* is the velocity potential at the boundary-layer displacement thickness. It is approximated by the velocity potential of a spherical source in a uniform stream

$$\Phi = v_x x - v_r r_s \quad (32)$$

where r_s is the local source spherical radius which is treated as equivalent to the local body radius (r_b). Then

$$\Phi_1^* - \Phi_2^* = -(v_{r_1} - v_{r_2})r_b \quad (33)$$

When the boundary-layer displacement thickness is treated as a physical boundary, the radial velocity difference is approximated by

$$v_{r_1} - v_{r_2} = V_\infty(\partial/\partial x)(\delta_1^* - \delta_2^*) \quad (34)$$

From Eqs. (29, 28, 31, 33, and 34) the pressure difference from side to side resulting from boundary-layer distortion is obtained

$$P_1 - P_2 = \rho_\infty r_b p V_\infty \sin\alpha\sin\phi(\delta/r_b)[(1.24/\beta) - (0.868/\beta)(pd/2V_\infty)^2(x/d)^2 + (0.985/\beta)(pd/2V_\infty)^4(x/d)^4] \quad (35)$$

after algebraic manipulation. The boundary-layer thickness δ is the compressible laminar thickness at zero spin and angle of attack.

The component of Magnus force caused by the radial pressure gradient is derived from the previously developed boundary-layer model and the Navier-Stokes equations for radial pressure gradient and the continuity equation, which are[9]

$$\rho\left(v_r\frac{\partial v_r}{\partial r} + \frac{v_\phi}{r}\frac{\partial v_r}{\partial\phi} - \frac{v_\phi^2}{r} + v_x\frac{\partial v_r}{\partial x}\right) = -\frac{\partial P}{\partial r} + \mu\left(\frac{\partial^2 v_r}{\partial r^2} + \frac{1}{r}\frac{\partial v_r}{\partial r} - \frac{v_r}{r^2} + \frac{1}{r^2}\frac{\partial^2 v_r}{\partial\phi^2} - \frac{2}{r^2}\frac{\partial v_\phi}{\partial\phi} + \frac{\partial^2 v_r}{\partial x^2}\right) \quad (36)$$

$$\frac{\partial v_r}{\partial r}+\frac{v_r}{r}+\frac{1}{r}\frac{\partial v_\phi}{\partial \phi}+\frac{\partial v_x}{\partial x}=0 \tag{37}$$

By using Eqs. (19–21) it is possible to integrate Eq. (37) over r, thereby obtaining an incompressible expression for v_r

$$v_r=-2V_\infty \sin\alpha\cos\phi[x/r(Re_x)^{1/2}]f+\tfrac{1}{2}[V_\infty/(Re_x)^{1/2}](\eta f'-f) \tag{38}$$

which includes the effects of crossflow as well as the longitudinal flow. This equation can be corrected for compressibility by multiplying by T'/T_∞ and it can be extended so that it is valid at large distances from the body by multiplying by r_b/r, which is indicated by the work of Seban and Bond.[15]

$$v_r=-2V_\infty \sin\alpha\cos\phi(r_b/r)[x/(Re_x)^{1/2}](T'/T_\infty)f+\tfrac{1}{2}[V_\infty/(Re_x)^{1/2}](T'/T_\infty)(r_b/r)(\eta f'-f) \tag{39}$$

While it will not be shown, the viscous terms on the right side of Eq. (36) were evaluated with Eqs. (39, 19, and 20) and found to be small enough to ignore. The centrifugal term $(\rho v_\phi{}^2/r)$ is by far the largest contributor and is

$$-\left[\frac{\partial P_1}{\partial r}-\frac{\partial P_2}{\partial r}\right]=\rho\left(\frac{v_{\phi_1}{}^2-v_{\phi_2}{}^2}{r}\right) \tag{40}$$

expressed in difference form. When Eqs. (19) and (20) are substituted for v_{ϕ_1} and v_{ϕ_2} in Eq. (40) and integrated

$$-\int_{r_b}^{\infty}\frac{\partial}{\partial r}(P_1-P_2)\,dr=8\rho' r_b\, pV_\infty \sin\alpha\sin\phi\,\frac{1}{r_b}\int_{r_b}^{\infty}[f'-f'^2]\,dr \tag{41}$$

where ρ is treated as the effective density ρ' shown in Eq. (5). Also notice that r is replaced by r_b because $[f'-f'^2]\simeq 0$ at the edge of the boundary layer where $r=r_b+\delta$, and since $\delta \ll r_b$, r can be approximated by a constant r_b. The differential dr can be obtained from Eq. (10) by assuming an undistorted boundary layer (i.e., $m_n=m_{\alpha,p}=1$) and noting that $y=r-r_b$

$$dr=[x/(Re_x)^{1/2}](T'/T_\infty)\,d\eta \tag{42}$$

Substituting Eq. (42) into Eq. (41) and completing the integration on the left side yields

$$P_1-P_2=8\rho' r_b\, pV_\infty \sin\alpha\sin\phi\,\frac{x}{(Re_x)^{1/2}}\left(\frac{T'}{T_\infty}\right)\frac{1}{r_b}\int_o^{\infty}[f'-f'^2]\,d\eta \tag{43}$$

since $[P_1-P_2]_\infty$ resulting from the upper limit approaches zero. The integral of $(f'-f'^2)\,d\eta$ was evaluated numerically and found to be 0.683. Consequently, Eq. (43) can be rewritten as

$$P_1-P_2=\frac{8(0.683)}{5.2}\rho' r_b\, pV_\infty \sin\alpha\times \sin\phi[5.2x/(Re_x)^{1/2}](T'/T_\infty)(1/r_b) \tag{44}$$

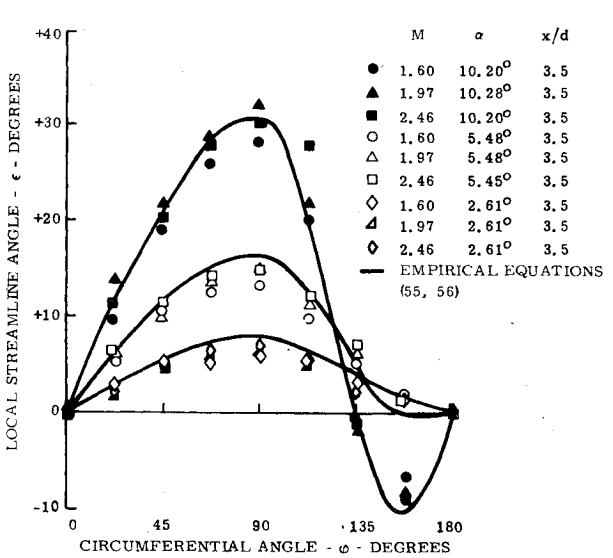

Fig. 9 Local inviscid streamline angle of ogive-cylinder afterbody determined from oil flow tests.

and from Eqs. (5) and (44)

$$P_1-P_2=1.051(T_\infty/T')\rho_\infty r_b\, pV_\infty \sin\alpha\sin\phi\,\delta/r_b \tag{45}$$

where δ is the compressible boundary-layer thickness undistorted by spin and angle of attack. This equation expresses the difference in pressure from side to side resulting from the centrifugal effect, except that a second-order error is involved in the derivation. It was, in effect, assumed that the volume or mass in the boundary layer was proportional to $(2\pi r_b\delta)$; however, it is more exactly proportional to $[\pi(r_b+\delta)^2-\pi r_b{}^2]$. Consequently, Eq. (45) should be multiplied by the ratio

$$[\pi(r_b+\delta)^2-\pi r_b{}^2]/2\pi r_b\delta=1+\tfrac{1}{2}\delta/r_b \tag{46}$$

so that

$$P_1-P_2=1.051(T_\infty/T')\rho_\infty r_b\, pV_\infty \sin\alpha\sin\phi(\delta/r_b)(1+\tfrac{1}{2}\delta/r_b) \tag{47}$$

which results in a second-order term in δ/r_b that would cause great complexity in the final equations. Since $\delta/2r_b \ll 1$ the dependence on δ/r_b can be reduced back to first order by assuming an average value of 0.08 (T'/T_∞) for δ/r_b which was estimated by calculating extreme values $(0.03<(\delta/r_b)<0.13)$ for wind-tunnel conditions. Then Eq. (47) becomes

$$P_1-P_2=[1.051(T_\infty/T')+0.04]\rho_\infty r_b\, pV_\infty \sin\alpha\sin\phi\,\delta/r_b \tag{48}$$

which is the final equation for the centrifugal effect. This predicts a centrifugal effect about three times that shown by Kelly.[5] The reason for this is unknown.

There are three other potential terms on the left side of Eq. (36) that can be evaluated[16] by using Eqs. (38, 19, and 20). Due to their small effect only the final result of evaluating these terms is shown. First the pressure differences associated with the term $v_r\partial r_v/\partial r$ is zero. The pressure difference associated with the term $(v_\phi/r)(\partial v_r/\partial_\phi)$ is

$$P_1-P_2=-0.104(T_\infty/T')\rho_\infty r_b\, pV_\infty \sin\alpha\sin\phi(\delta/r_b)^2 \tag{49}$$

which, when reduced to first order in δ/r_b by the same technique discussed above becomes

$$P_1-P_2=-0.0083\rho_\infty r_b\, pV_\infty \sin\alpha\sin\phi\,\delta/r_b \tag{50}$$

The magnitude of this term is practically insignificant $(<1\%)$ compared to the total pressure difference. The contribution of the last term $v_x(\partial v_r/\partial x)$ is significant $(\sim 11\%$ of the total) and is

$$P_1-P_2=[0.006+0.248(T_\infty/T')]\rho_\infty r_b\, pV_\infty \sin\alpha\sin\phi\,\delta/r_b \tag{51}$$

after reduction to first order in δ/r_b. A complete development of these terms is given in Ref. 16.

The total pressure difference from side to side is obtained by adding Eqs. (35, 48, 50, and 51) which is

$$P_1-P_2=\{1.30(T_\infty/T')+0.04+[1-0.23(pd/2V_\infty)^2L^2+0.0159(pd/2V_\infty)^4L^4]1.24/\beta\}\rho_\infty r_b\, pV_\infty \sin\alpha\sin\phi\,\delta/r_b \tag{52}$$

where the average value of $(x/d)^2$ and $(x/d)^4$ were obtained from

$$\left(\frac{x}{d}\right)^2_{\text{ave}}=\frac{1}{l}\int_0^l\left(\frac{x}{d}\right)^2 dx=\frac{1}{3}\left(\frac{l}{d}\right)^2=\frac{1}{3}L^2 \tag{53}$$

$$\left(\frac{x}{d}\right)^4_{\text{ave}}=\frac{1}{l}\int_0^l\left(\frac{x}{d}\right)^4 dx=\frac{1}{5}\left(\frac{l}{d}\right)^4=\frac{1}{5}L^4 \tag{54}$$

This simplification greatly reduces the complexity of the final equations without introducing significant error, because the higher order terms in $pd/2V_\infty$ are normally small.

The next step is to modify the circumferential inviscid velocity caused by crossflow to account for vortex formation on the leeside of the afterbody. Figure 9 shows the local inviscid streamline angle measured[8] with oil flow techniques on a three caliber cylindrical afterbody with a two caliber tangent ogive nose. These are believed to be the approximate streamline angles $(\varepsilon \simeq v_{\phi i}/V_\infty)$ to be found at the edge of the boundary layer, because the oil droplet diameter appears to be large enough compared to the boundary-layer thickness so that the droplet trajectory is primarily a function of the velocity at the edge of the boundary layer. While the streamline angle measurements shown were made at the midpoint of the afterbody, the angle did not seem to be very sensitive to body station, at least at small angles of attack. From these data, it was possible to arrive at an empirical relationship for the inviscid circumferential velocity, which is

$$(v_{\phi_i})_a = 3V_\infty \sin\alpha \sin\phi, \quad 0 \leqq \phi \leqq \pi/2 \tag{55}$$

$$(v_{\phi_i})_a = 3V_\infty \sin\alpha(\sin\phi + |\alpha|[4.05\sin 2\phi + 1.15\sin 4\phi]), \quad \pi/2 \leqq \phi \leqq \pi \tag{56}$$

Now let

$$h = \{1.30(T_\infty/T') + 0.04 + [1 - 0.23(pd/2V_\infty)^2 L^2 + 0.0159(pd/2V_\infty)^4 L^4]\, 1.24/\beta\} \tag{57}$$

Then Eq. (52) becomes

$$[P_1 - P_2]_n = (h/2)\rho_\infty r_b p(2V_\infty \sin\alpha \sin\phi)(\delta_n/r_b), \quad 0 \leqq \phi \leqq \pi \tag{58}$$

which is the pressure difference on the nose. Also, $(2V_\infty \sin\alpha \sin\phi)$ is the inviscid circumferential velocity obtained from potential flow which is known from the oil flow tests[8] to be an adequate representation on the nose. Now Eqs. (55) and (56) are substituted for $2V_\infty \sin\alpha \sin\phi$ in Eq. (58) to obtain the pressure difference on the afterbody

$$[P_1 - P_2]_a = (h/2)\rho_\infty r_b p(3V_\infty \sin^\alpha \sin\phi(\delta_a/r_b), \quad 0 \leqq \phi \leqq \pi/2 \tag{59}$$

$$[P_1 - P_2]_a = (h/2)\rho_\infty r_b p[3V_\infty \sin\alpha(\sin\phi + |\alpha|[4.05\sin 2\phi + 1.15\sin 4\phi])](\delta_a/r_b), \quad \pi/2 \leqq \phi \leqq \pi \tag{60}$$

It should be noted that for a strictly rigorous approach, the substitution of Eqs. (55) and (56) should be done earlier in the derivation. However, the present method is simpler and results in an insignificant error because it only affects the second-order terms.

The Magnus force is obtained by integrating the pressure difference equations over the body surface area

$$F_y = -\int_{x=0}^{x=l_n}\int_{\phi=0}^{\phi=\pi} [P_1 - P_2]_n r_b \sin\phi\, d\phi\, dx - \int_{x=l_n}^{x=l}\int_{\phi=0}^{\phi=\pi} [P_1 - P_2]_a r_b \sin\phi\, d\phi\, dx \tag{61}$$

where l_n is the nose length. Substituting Eqs. (58–60) in Eq. (61) and integrating over ϕ yields

$$F_y = -\frac{\pi}{4} h\rho_\infty p V_\infty \sin\alpha \left\{2\int_{x=o}^{x=l_n} \delta_n r_b\, dx + 3(1 - 1.52|\alpha|)\int_{x=l_n}^{x=l} \delta_a r_b\, dx\right\} \tag{62}$$

The Magnus force coefficient is defined as

$$C_{y_{p\alpha}} = \frac{F_y}{\frac{1}{2}\rho_\infty V_\infty{}^2 (pd/2V_\infty)(\pi/4) d^2 \alpha} \tag{63}$$

Substituting Eq. (62) in Eq. (63) yields

$$C_{y_{p\alpha}} = -\frac{4h}{d^3}\left\{2\int_{x=o}^{x=l_n} \delta_n r_b\, dx + 3(1 - 1.52|\alpha|)\int_{x=l_n}^{x=l} \delta_a r_b\, dx\right\} \tag{64}$$

when it is assumed that $\alpha \simeq \sin\alpha$. The Magnus moment equation is simply

$$C_{n_{p\alpha}} = \frac{4h}{d^4}\left\{2\int_{x=o}^{x=l_n} \delta_n r_b x\, dx + 3(1 - 1.52|\alpha|)\int_{x=l_n}^{x=l} \delta_a r_b x\, dx\right\} \tag{65}$$

where the moment is referenced to the nose. Note that the integrands are functions of the local compressible boundary-layer thickness (δ) at zero angle of attack and spin and the local body radius (r_b). The local body radius for the tangent ogive is given by Eq. (11) and for a cone is

$$r_b = (x/2)\, d/l_c \quad \text{(cone)} \tag{66}$$

The boundary-layer thickness for a tangent ogive cylinder is obtained from Eqs. (10) and (13)

$$\delta_{n,o} = \frac{5.2x}{(Re_x)^{1/2}}\left(\frac{T'}{T_\infty}\right)\left[(3)^{1/2} - \frac{x_o}{l_o}\left(\frac{(3)^{1/2} - 1}{2}\right)\right]^{-1} \quad \text{(ogive nose)} \tag{67}$$

$$\delta_a = [5.2x/(Re_x)^{1/2}](T'/T_\infty) \quad \text{(afterbody)} \tag{68}$$

where $\eta = 5.2$. The equations for a cone cylinder are

$$\delta_{n,c} = [5.2x/(Re_x)^{1/2}](T'/T_\infty)/(3)^{1/2} \quad \text{(cone nose)} \tag{69}$$

$$\delta_a = [5.2x/(Re_x)^{1/2}](T'/T_\infty) \quad \text{(afterbody)} \tag{70}$$

$$\delta_c = [5.2x/(Re_x)^{1/2}](T'/T_\infty)[1/(3)^{1/2}]\, V_c/V_\infty \quad \text{(cone body)} \tag{71}$$

which is identical to the conical nose equation, except that the ratio of cone surface velocity to freestream velocity has been included because it is a significant correction in the case of blunt cones.

When the equations for the local body radius and the local boundary-layer thickness are substituted into Eqs. (64) and (65) and integrated, the following equations for the Magnus force and moment result.

Ogive cylinder:

$$[C_{y_{p\alpha}}]_{oc} = -\frac{20.80H(1 - 1.52|\alpha|)}{(Re_l)^{1/2}} L^2 \times \left\{1 - \left[1 - \frac{0.366}{1 - 1.52|\alpha|}\right]\left(\frac{L_o}{L}\right)^{3/2}\right\} \tag{72}$$

$$[C_{n_{p\alpha}}]_{oc} = \frac{12.48H(1 - 1.52|\alpha|)}{(Re_l)^{1/2}} L^3 \times \left\{1 - \left[1 - \frac{0.407}{1 - 1.52|\alpha|}\right]\left(\frac{L_o}{L}\right)^{5/2}\right\} \tag{73}$$

Cone cylinder:

$$[C_{y_{p\alpha}}]_{cc} = -\frac{20.80H(1 - 1.52|\alpha|)}{(Re_l)^{1/2}} L^2 \times \left\{1 - \left[1 - \frac{0.231}{1 - 1.52|\alpha|}\right]\left(\frac{L_c}{L}\right)^{3/2}\right\} \tag{74}$$

$$[C_{n_{p\alpha}}]_{cc} = \frac{12.48H(1 - 1.52|\alpha|)}{(Re_l)^{1/2}} L^3 \times \left\{1 - \left[1 - \frac{0.275}{1 - 1.52|\alpha|}\right]\left(\frac{L_c}{L}\right)^{5/2}\right\} \tag{75}$$

where H is

$$H = 1.30 + 0.04(T'/T_\infty) + [1 - 0.23(pd/2V_\infty)^2 L^2 + 0.0159(pd/2V_\infty)^4 L^4](1.24/\beta)(T'/T_\infty) \tag{76}$$

$$T'/T_\infty = 1 + 0.1224 M_\infty{}^2, \quad \text{(wind-tunnel conditions)} \tag{77}$$

Cone:

$$[C_{y_{p\alpha}}]_c = -\frac{4.80H_c}{(Re_{l_c})^{1/2}}\left(\frac{V_c}{V_\infty}\right) L_c{}^2 \tag{78}$$

$$[C_{n_{p\alpha}}]_c = \frac{3.43H_c}{(Re_{l_c})^{1/2}}\left(\frac{V_c}{V_\infty}\right) L_c{}^3 \tag{79}$$

where

$$H_c = 1.30 + 0.04(T'/T_\infty)_c + [1 - 0.23(pd/2V_\infty)^2 L_c{}^2 + 0.0159(pd/2V_\infty)^4 L_c{}^4](1.24/\beta)(T'/T_\infty) \tag{80}$$

$$T'/T_\infty = 1 + 0.1224 M_c{}^2, \quad \text{(wind-tunnel conditions)} \tag{81}$$

For flight conditions (T'/T_∞) should be obtained from Eq. (7). The approximations used for the integral over the nose of the ogive cylinder are discussed in detail in Ref. 16. A similar derivation including boundary-layer transition from laminar to turbulent flow, which is too lengthy to be presented in this paper, is shown in Ref. 16.

IV. Comparison of Theory and Experiment

The theory for the Magnus force coefficient for an ogive cylinder [Eq. (72)] and center of pressure, obtained by dividing Eq. (73) by Eq. (72) and reversing sign, is compared in Table 1 with experimental data[4] obtained under laminar flow conditions at supersonic Mach numbers. The agreement is excellent at the low supersonic Mach numbers but is only fair at the higher Mach numbers where the theory seems to consistently underestimate the Magnus force. The theoretical center of pressure, which is only a function of projectile shape, agrees well with the average experimental values. The Magnus force center of pressure is very difficult to measure experimentally and individual data points are likely to be in error.

Table 1 Comparison of theory with experimental Magnus force coefficient data for a tangent ogive-cylinder in supersonic flow

Ogive-cylinder, $L_o = 1.506$, $L = 3.206$ (exp. data from Platou)[4]

M_∞	$Re_l^a \times 10^{-6}$	$C_{Y_{p_{ex}}}$ Exp.	$C_{Y_{p_{th_{oc}}}}$ Theory	$C_{Y_{p_{ex}}}$ % Error	x_{cp}/d Exp.	x_{cp}/d Theory	x_{cp}/d % Error
1.57	2.421	−0.281	−0.294	+4.6	2.46	2.20	−10.7
2.00	2.068	−0.276	−0.287	+4.0	2.21	2.20	−0.2
2.47	2.068	−0.321	−0.276	−14.0	1.96	2.20	+12.2
3.02	2.068	−0.337	−0.273	−19.0	2.21	2.20	−0.2

Ogive-cylinder, $L_o = 1.506$, $L = 5.000$ (exp. data from Platou)[4]

M_∞	$Re_l^a \times 10^{-6}$	$C_{Y_{p_{ex}}}$ Exp.	$C_{Y_{p_{th_{oc}}}}$ Theory	$C_{Y_{p_{ex}}}$ % Error	x_{cp}/d Exp.	x_{cp}/d Theory	x_{cp}/d % Error
1.75	1.823	−0.88	−0.876	−0.5	3.25	3.25	0
2.00	1.647	−0.75	−0.880	+17.3	3.00	3.25	+8.3
3.00	1.518	−0.97	−0.871	−10.2	2.75	3.25	+18.2

[a] Re_l based on total length instead of effective length used in Ref. 4.

The Magnus force coefficients calculated by the present theory for tangent ogive cylinders of two different lengths in laminar flow at a low subsonic Mach number ($M_\infty = 0.2$) is shown in Fig. 10 compared with experimental data obtained from Fletcher.[17] The theory and data are in fair agreement and the nonlinearity as a function of spin rate seems to be adequately predicted by the theory even for these relatively long bodies ($L = 5.90$ and 7.07) at a moderately high angle of attack ($\alpha = 10°$).

The theory is compared with experimental data obtained from Curry et al.[18] on a 10° cone tested under laminar conditions at a Mach number of 3.02 (Fig. 11). The theory and data are in good agreement up to the maximum angle of attack of 10°. The theory of Sedney[7] is shown for comparison.

V. Discussion

Some observations regarding the Magnus physical phenomena can be made from the theory. Referring to Eq. (62) it can be seen that the Magnus force is directly proportional to the boundary-layer thickness and local body radius. The effect of body radius can be deduced from Eq. (74), where it can be shown that for a cone cylinder body with equal nose and afterbody lengths, the conical nose only contributes 31% of the total force. Consequently, the nose will contribute very little to the Magnus force acting on long bodies with short noses. The Magnus coefficients are proportional to the square of the fineness ratio (L) of the body and the reciprocal of the square root of Reynolds number based on body length, which coincides with previous theoretical work.

Two explicit nonlinear effects appear in the theory. The first, which is a function of angle of attack, is due to the formation of leeside vortices and is a likely explanation for the fact that a

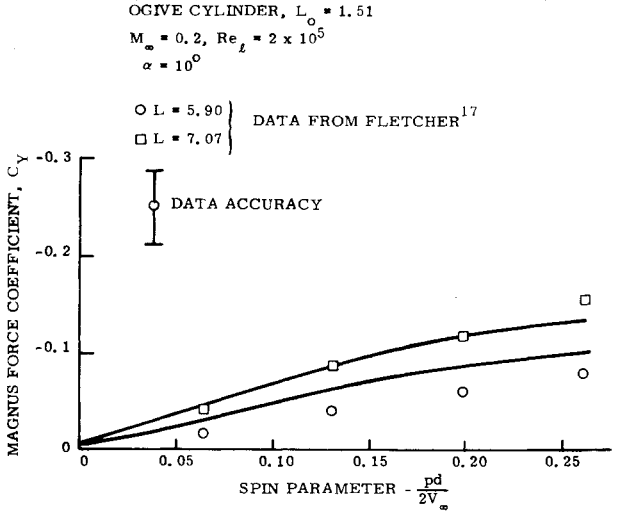

Fig. 10 Comparison of theory and experimental Magnus force coefficient for tangent ogive-cylinder bodies in subsonic flow.

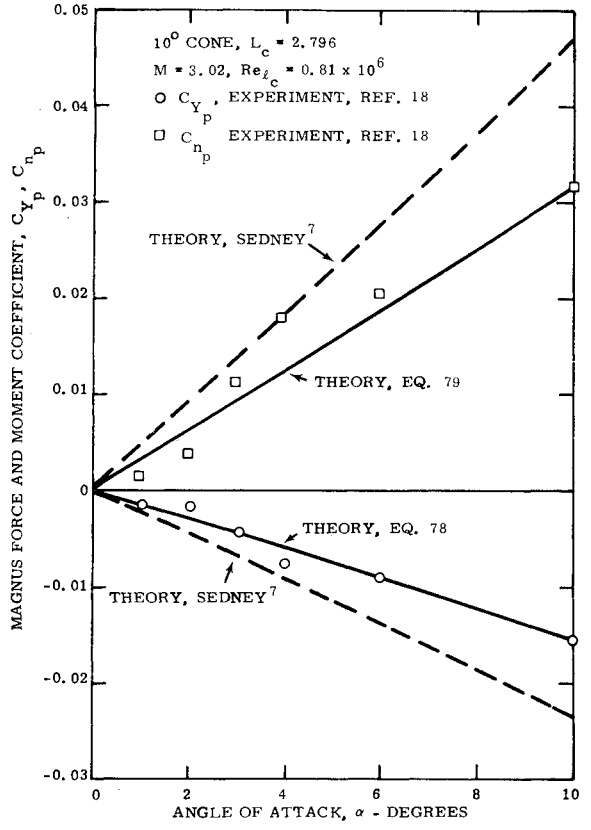

Fig. 11 Comparison of theory with experimental Magnus data for a cone in supersonic flow.

peak in Magnus coefficients is often observed[19] to occur in the vicinity of 19° angle of attack. The theory predicts that a peak in the Magnus force should occur at 18.9°. The second nonlinearity, which results from boundary-layer distortion, is the nonlinear dependence on the spin parameter. This nonlinear phenomenon has little effect unless fairly large values of the spin parameter and fairly long bodies are involved.

Two nonlinear effects are implied by virtue of the fact that the Magnus force is proportional to the boundary-layer thickness and that use of the Blasius solution assumes that an attached boundary-layer is present. Transition from a laminar to a turbulent boundary layer, which was investigated in Ref. 16, can result in a very strong nonlinear effect, because the boundary-layer thickness and Magnus force increases drastically as transition moves forward on the body with increasing angle of attack. Boundary-layer separation, which is not investigated in this theory, may cause a drastic reduction in the Magnus force, although this remains to be proven.

The theory starts deteriorating at values of the product of angle of attack and fineness ratio ($\alpha \cdot L$) much above unity, which for a 6 caliber body occurs at approximately 10° angle of attack. Also, the accuracy can be expected to be poor for either very short or very long bodies which tend to violate the assumptions used in deriving the theory.

VI. Conclusions

A Magnus theory has been derived which agrees favorably with experimental data obtained under conditions that are compatible with the assumptions. A large increase in Magnus coefficients in the transonic region is predicted by the theory, which could cause a transonic instability of spin stabilized projectiles. The Magnus coefficients are shown to be directly proportional to the boundary-layer thickness, which implies that the Magnus force and moment are much larger in the case of a turbulent boundary layer than for a laminar boundary layer. The presence of leeside vortices on the afterbody causes a nonlinear Magnus coefficient behavior in terms of angle of attack. The theory predicts a maximum in Magnus coefficients occurring at approximately 19° angle of attack. The projectile wall temperature has a significant effect on the Magnus coefficients occurring in flight.

References

[1] Murphy, C. H., "Free Flight Motion of Symmetric Missiles," Rept. 1216, July 1963, Ballistic Research Labs., Aberdeen Proving Ground, Md.

[2] Nicolaides, J. D., "On the Free Flight Motion of Missiles Having Slight Configurational Asymmetries," Rept. 858, June 1953, Ballistic Research Labs., Aberdeen Proving Ground, Md.

[3] Vaughn, H. R., "A Detailed Development of the Tricyclic Theory," SC-M-67-2933, Feb. 1968, Sandia Labs., Albuquerque, N. Mex.

[4] Platou, A. S., "Magnus Characteristics of Finned and Nonfinned Projectiles," *AIAA Journal*, Vol. 3, No. 1, Jan. 1965, pp. 83–90.

[5] Kelly, H. R. and Thacker, R. G., "The Effect of High Spin on the Magnus Force on a Cylinder at Small Angles of Attack," NAVORD Rept. 5036, Feb. 1956, Naval Ordnance Lab., White Oak, Md.

[6] Martin, J. C., "On Magnus Effects Caused by the Boundary Layer Displacement Thickness on Bodies of Revolution at Small Angles of Attack," Rept. 870, June 1955, Ballistic Research Labs., Aberdeen Proving Ground, Md.

[7] Sedney, R., "Laminar Boundary Layer on a Spinning Cone at Small Angles of Attack," Rept. 991, Sept. 1956, Ballistic Research Labs., Aberdeen Proving Ground, Md.

[8] Vaughn, H. R. and George, O. L., "Surface Flow Angles on an Ogive Cylinder at Angle of Attack in Supersonic Flow," SC-RR-71 0781, Dec. 1971, Sandia Labs., Albuquerque, N. Mex.

[9] Schlichting, H., *Boundary Layer Theory*, McGraw-Hill, New York, 1968.

[10] Blottner, F. G., "Finite Difference Methods for Solution of the Boundary-Layer Equations," *AIAA Journal*, Vol. 8, No. 2, Feb. 1970, pp. 193–205.

[11] Eckert, E. R. G., "Engineering Relations for Friction and Heat Transfer in High Velocity Flow," *Journal of the Aeronautical Sciences*, Aug. 1955.

[12] Vaughn, H. R. and George, O. L., "Experimental and Theoretical Investigation of a Laminar Boundary Layer on a Spinning Tangent Ogive Cylinder at Angle of Attack," SC-RR-71 0851, March 1972, Sandia Labs., Albuquerque, N. Mex.

[13] Funuya, Y. and Nakamura, I., "Velocity Profiles in the Skewed Boundary Layers on Some Rotating Bodies in Axial Flow," *Journal of Applied Mechanics*, March 1970, pp. 17–24.

[14] Kuethe, A. M. and Schetzer, T. D., *Foundations of Aerodynamics*, Wiley, New York, 1959.

[15] Seban, R. A. and Bond, R., "Skin Friction and Heat Transfer Characteristics of a Laminar Boundary Layer on a Cylinder in Axial Incompressible Flow," *Journal of the Aeronautical Sciences*, Oct. 1951.

[16] Vaughn, H. R. and Reis, G. E., "A Magnus Theory for Bodies of Revolution," SC-RR-72 0537, Sept. 1972, Sandia Labs., Albuquerque, N. Mex.

[17] Fletcher, C. A. J., "The Magnus Characteristics of a Spinning Inclined Ogive Cylinder Body at Subcritical Reynolds Numbers in Incompressible Flow," WRE Rept. 423, June 1971, Weapons Research Establishment, Salisbury, South Australia.

[18] Curry, W. H., Platou, A. S., and Reynolds, W. C., "Magnus Characteristics of a 10° Cone at Supersonic Mach Numbers," Sandia Labs., Rept. (to be published).

[19] Luchuk, W., "The Dependence of the Magnus Force and Moment on the Shape of Cylindrical Bodies of Fineness Ratio 5 at a Mach Number of 1.75," NAVORD 4425, 1957, Naval Ordnance Lab., White Oak, Md.